

Research Article

Bo Zhao, Valeria Rodríguez-Fajardo, Xiao-Bo Hu, Raul I. Hernandez-Aranda, Benjamin Perez-Garcia*, and Carmelo Rosales-Guzmán†

Parabolic-accelerating vector waves

<https://doi.org/10.1515/sample-YYYY-XXXX>

Received Month DD, YYYY; revised Month DD, YYYY; accepted Month DD, YYYY

Abstract: Complex vector light fields have become a topic of late due to their exotic features, such as their non-homogeneous transverse polarisation distributions and the non-separable coupling between their spatial and polarisation degrees of freedom. In general, vector beams propagate in free space along straight lines, being the Airy-vector vortex beams the only known exception. Here, we introduce a new family of vector beams that exhibit novel properties that have not been observed before, such as their ability to freely accelerate along parabolic trajectories. In addition, their transverse polarisation distribution only contains polarisation states oriented at exactly the same angle but of different ellipticity. We anticipate that these novel vector beams might not only find applications in fields such as optical manipulation, microscopy or laser material processing, but extend to others.

Keywords: Vector beams, accelerating waves, structured light.

1 Introduction

The ingrained notion that light travels along a straight line was first defied in 2007 by Siviloglou *et al.* [1], who introduced a novel kind of light beam with the ability to self-accelerate along a parabolic trajectory upon free space propagation [2]. Such light beams, known as Airy beams, are natural solutions of the normalised paraxial wave equation. Crucially, even though they seem to prop-

agate along parabolic trajectories, their centroid propagates along straight lines, in accordance to the electromagnetic momentum conservation law. Along with the discovery of Airy beams, their fascinating properties prompted the development of novel applications, which have impacted a wide diversity of fields, such as, optical manipulation, microscopy, laser material processing, among others (see for example [3] for an extensive review). More importantly, the experimental demonstration of Airy beams ignited the quest for other kinds of accelerating beams [4–11]. Of particular interest is the case of accelerating parabolic beams, which form a complete and infinite orthogonal family of solutions of the normalised paraxial wave equation [4, 12]. Such beams also propagate in free space in a non diffracting way describing parabolic trajectories.

Noteworthy, most of the work carried out with accelerating beams has only considered the case of homogeneously polarised beams, while the manipulation of other degrees of freedom is gaining popularity, giving rise to a more general class of beams generally known as structured light fields. This is the case of complex vector light beams, classically-entangled in their spatial and polarisation degrees of freedom, which feature a non-homogeneous polarisation distribution across the transverse plane [13–15]. Such beams have gained popularity in recent time not only due to their unique traits, such as their quantum-like non separability [16–20], but also due to the many applications they are pioneering [21–26]. In vector beams, their spatial and polarisation degrees of freedom are coupled in a non-separable way, which generates the non-homogeneous polarisation distribution. Importantly, while the polarisation degree of freedom is restricted to a two-dimensional space, the spatial one is not, as any of the unbounded solution sets of the wave equation, either in its exact or paraxial version, can be used. Examples of vector beams that have been experimentally demonstrated are Bessel, Laguerre-, Ince- and Mathieu-Gauss beams, amongst others, all of which propagate along straight trajectories [27–31]. Along this line, previous works have demonstrated the acceleration of vectorial fields, in which case, their polarisation structures rotates around the optical axis, while still propagate along

Bo Zhao, Xiao-Bo Hu, Carmelo Rosales-Guzmán†, Wang Da-Heng Collaborative Innovation Center, Heilongjiang Provincial Key Laboratory of Quantum Manipulation and Control, Harbin University of Science and Technology, Harbin 150080, China
Raul I. Hernandez-Aranda, Benjamin Perez-Garcia, Photonics and Mathematical Optics Group, Tecnológico de Monterrey, Monterrey 64849, Mexico, e-mail: b.pegar@tec.mx
Valeria Rodríguez-Fajardo, School of Physics, University of the Witwatersrand, Private Bag 3, Johannesburg 2050, South Africa
Carmelo Rosales-Guzmán†, Centro de Investigaciones en Óptica, A.C., Loma del Bosque 115, Colonia Lomas del campestre, 37150 León, Gto., Mexico, e-mail: carmelorosalesg@cio.mx

straight lines [32]. Perhaps the only known case of a vector beam capable to propagate along a parabolic trajectory is the Airy-vortex vector beam [33].

We propose and experimentally demonstrate a new family of vector beams, which we term Accelerating Vector Waves (AVWs), that are non-separable weighted superpositions of the polarisation and spatial degrees of freedom encoded in the orthogonal set of accelerating waves. These beams exhibit two interesting properties, namely, that their non-homogeneous polarisation distributions propagate in free space along parabolic trajectories maintaining a maximum degree of coupling, and that, even though the non-homogeneous transverse polarisation distribution of an individual AVW contains different states of elliptical polarisation, all of them are located on a great circle on the Poincaré sphere representation for polarisation. Here, we start by describing these beams theoretically, then move to their implementation in the laboratory, and finally show experimental results to showcase their novel features. Due to their intriguing properties, we expect AVWs will attract the wide interest of the optical community, stemming not only from their potential applications but also from their fundamental aspects.

2 Theory

Accelerating parabolic waves (APWs) are solutions of the paraxial wave equation in parabolic coordinates. They are non-diffracting beams that accelerate during free-space propagation. Their experimentally realisable finite-energy form is given by [4]

$$\phi_n(\eta, \xi, z) = \exp[i(z/2k\kappa^2 - ia)(\eta^2 - \xi^2)/2] \times \exp[i(z/2k\kappa^2 - ia)^3/3] \Theta_n(\eta) \Theta_n(i\xi), \quad (1)$$

where the parabolic coordinates (η, ξ) are related to the Cartesian coordinates by $(\eta^2/2 - \xi^2/2, \eta\xi) = (x/\kappa - (z/2\kappa^2)^2 + ia z/k\kappa^2, y/\kappa)$, κ is a transverse scale parameter, k is the wave number, z is the propagation distance and a is parameter that controls the exponential aperture of the beam at $z = 0$. The functions $\Theta_n(\cdot)$ correspond to the solutions of the differential equation

$$\left(-\frac{1}{2} \frac{d^2}{d\eta^2} + \frac{\eta^4}{4}\right) N(\eta) = E N(\eta), \quad (2)$$

which corresponds to the one-dimensional Schrödinger equation with potential $V(\eta) = \eta^4/4$ (known as quartic potential) and $m = \hbar = 1$ [34]. Importantly, the eigen-solutions Θ_n ($n \in \mathbb{N}$) of Eq. 2 form an orthogonal set of functions, whose parity is governed by n . Since these

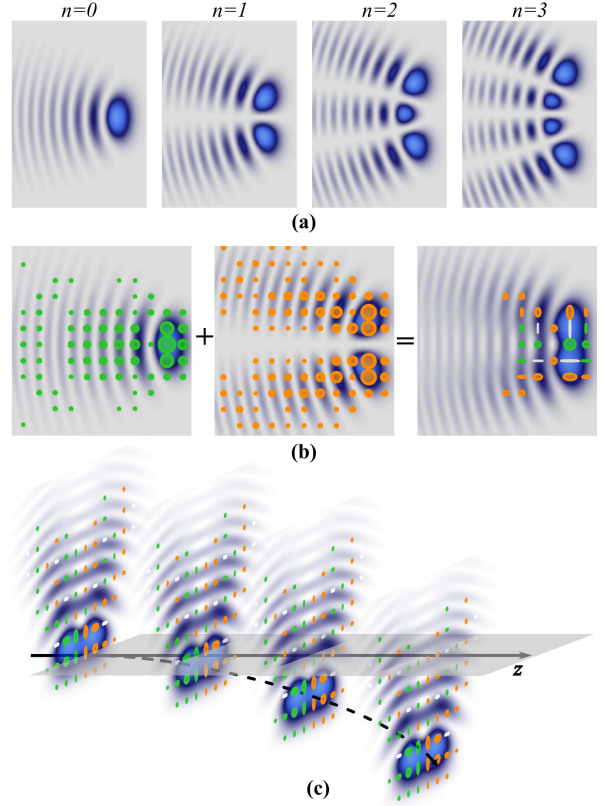


Fig. 1: (a) Intensity profiles of accelerating parabolic scalar waves of orders $n = \{0, 1, 2, 3\}$. (b) Schematic representation of the non-separable superposition of two orthogonal scalar modes carrying orthogonal polarisations to generate an accelerating vector wave $\mathbf{AVW}_{n,m}(\eta, \xi, z)$. (c) Illustration of the free-space propagation trajectory of an AVW along the z axis. Green and orange ellipses represent right- and left-handed circular polarisation, respectively, and white lines represent linear polarisation.

eigen-solutions cannot be expressed in a closed form, a suitable numerical method must be employed to obtain them [35]. In particular, we are interested in square integrable eigen-solutions of Eq. 2. Fig. 1(a) shows the intensity profiles of the scalar APWs for $n = \{0, 1, 2, 3\}$. As can be seen, for $n = 0$ the intensity profile of the beam contains only one main lobe of maximum intensity and additional subsequent lobes of decaying intensity. In general, for $n > 0$ the intensity profile is formed by $n + 1$ lobes of maximum intensity.

Mathematically, the accelerating Vector Waves (AVWs) are constructed as a superposition of two scalar APWs with orthogonal polarisations, such that at the z -

plane and for indices n, m they are given by

$$\begin{aligned} \mathbf{AVW}_{n,m}(\eta, \xi, z) = & \cos \alpha \phi_n(\eta, \xi, z) \hat{\mathbf{e}}_1(\theta, \varphi) + \\ & \sin \alpha \exp(i\beta) \phi_m(\eta, \xi, z) \hat{\mathbf{e}}_2(\theta, \varphi), \end{aligned} \quad (3)$$

where the weighting factor $\alpha \in [0, \pi/2]$ allows the field to change from scalar to vector, and the parameter $\beta = [0, \pi]$ controls the inter-modal phase. The basis vectors

$$\hat{\mathbf{e}}_1(\theta, \varphi) = \cos(\theta/2) \hat{\mathbf{e}}_R + \exp(i\varphi) \sin(\theta/2) \hat{\mathbf{e}}_L, \quad (4)$$

$$\hat{\mathbf{e}}_2(\theta, \varphi) = \sin(\theta/2) \hat{\mathbf{e}}_R - \exp(i\varphi) \cos(\theta/2) \hat{\mathbf{e}}_L, \quad (5)$$

represent the general elliptical polarisation basis. Note that we can obtain the left/right-handed circular polarisation basis by setting $\theta = \pi$ and $\varphi = 0$ and the horizontal/vertical basis with $\theta = \pi/2$ and $\varphi = 0$. Without loss of generality, here we will restrict our results to the circular polarisation basis, only briefly mentioning some theoretical examples of the horizontal/vertical basis. Fig. 1(b) illustrates conceptually the above description for the specific case $\mathbf{AVW}_{0,1}(\eta, \xi, z)$ with $\alpha = \pi/4$ and $\beta = 0$ as polarisation distributions overlay onto their corresponding intensity profiles. Left and middle panels show the two scalar modes $\theta \phi_n(\eta, \xi, z) \hat{\mathbf{e}}_L$ and $\phi_m(\eta, \xi, z) \hat{\mathbf{e}}_R$ with Right Circular polarisation (RCP) and Left Circular Polarisation (LCP), respectively, represented by green and orange ellipses for the first and second case respectively. Notice the intensity patterns of the scalar modes are different, as required to obtain vector modes. In a similar way, the right panel presents the non-separable superposition of both scalar modes (Eq. 3). The parabolic trajectory described by AVWs can be seen schematically in Fig. 1(c) for $\mathbf{AVW}_{2,3}(\eta, \xi, z)$ propagating along the z axis. Mathematically, this is expressed in the transverse shift $y_s = [z/(2k)]^2/\kappa^3$ [36], which is independent of the indices n, m .

3 Experimental details

We implemented the AVW described above using a Digital Micromirror Device (DMD) and following the technique that we proposed and fully characterised in a previous article [37]. This device is polarisation-insensitive, very flexible and versatile, allowing the generation of vector modes with arbitrary spatial distributions, such as elliptical or parabolic [30, 31, 37, 38]. In essence, a DMD is illuminated with two modes carrying orthogonal polarisations, impinging at slightly different angles but exactly at the geometric centre of the hologram displayed on

the DMD. The hologram contains a superposition of the two transmittance functions that generate the constituting scalar modes of Eq. 3, each with an additional unique linear spatial grating that redirects the mode along a specific angle, and whose periods are carefully chosen to guarantee both generated beams co-propagate along the same axis, where the desired vector beam is created. Transmittance functions are calculated as the inverse Fourier transform of the desired modes $\phi_n(\eta, \xi, z)$ [12, 36], thus we add a lens in a $2f$ configuration, where f is the focal length of the lens ($f = 200$ mm in our case), and measure at its back focal plane. Intensity patterns of the generated beams were captured with a high resolution CCD camera (FL3-U3-120S3C-C with resolution of 4000×3000 pixels and a pixel size of $1.55 \mu\text{m}$). Polarisation reconstruction was achieved through Stokes polarimetry, using a set of intensity measurements as detailed in [31]. Fig. 2(a) shows an example of the experimentally measured Stokes parameters S_0, S_1, S_2 and S_3 for the specific mode $\mathbf{AVW}_{1,2}(\eta, \xi, z = 0)$. Reconstructed intensity and polarisation distributions of a set of representative examples of the experimentally generated $\mathbf{AVW}_{n,m}(\eta, \xi, z = 0)$ modes using the circular polarisation basis are presented in Fig. 2(b), both for the theory (top row) and the experiment (bottom row). Notice the high similarity between the latter, demonstrating the good performance of our generation method.

4 Results and discussion

The vector modes described by equation 3 and shown in Fig. 2 propagate along parabolic trajectories maintaining not only their intensity and polarisation distribution but also a maximum coupling between both. We corroborated this by tracking the transverse spatial coordinates (x, y) of one of the lobes of maximum intensity as function of their propagation distance z . We observed that while the x coordinate remains almost constant, the y coordinate shifts following a quadratic trend. Figure 3, in which the coordinate y is plotted against the propagation distance z , clearly shows such behaviour for a representative set of AVWs given by $\mathbf{AVW}_{0,2}(\eta, \xi, z)$, $\mathbf{AVW}_{1,2}(\eta, \xi, z)$ and $\mathbf{AVW}_{2,3}(\eta, \xi, z)$. Since all modes shown were generated with the same initial parameters k and κ , they accelerated in an identical way. Insets show examples of the polarisation distribution overlapped with the intensity distribution at three propagation distances $z = 0$ mm, $z = 20$ mm and $z = 60$ mm for the mode $\mathbf{AVW}_{1,2}(\eta, \xi, z)$.

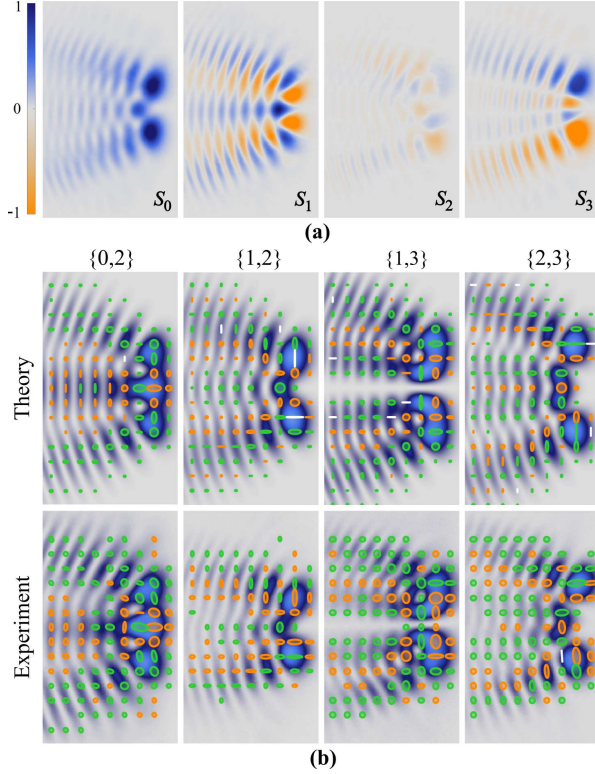


Fig. 2: (a) Example of experimentally measured Stokes parameters S_0 , S_1 , S_2 and S_3 for $\text{AVW}_{1,2}(\eta, \xi, z=0)$. (b) Theoretical and experimental reconstructed intensity and polarisation distribution from the Stokes parameters for the modes $\text{AVW}_{0,2}(\eta, \xi, 0)$, $\text{AVW}_{1,2}(\eta, \xi, 0)$, $\text{AVW}_{1,3}(\eta, \xi, 0)$ and $\text{AVW}_{2,3}(\eta, \xi, 0)$.

As mentioned earlier, AVWs can be generated with arbitrary degrees of non-separability, evolving from scalar to vector, via the parameter α (see Eq. 3). More precisely, as α increases from 0 to $\pi/4$ the mode changes monotonically from a pure scalar mode with right-handed circular polarisation ($\alpha = 0$) to a pure scalar mode with left-handed circular polarisation ($\alpha = \pi/2$), passing through a pure vector mode ($\alpha = \pi/4$). Intermediate values of α produce vector modes with intermediate degrees of non-separability, which can be measured through the concurrence or Vector Quality Factor (VQF), which is a measure borrowed from quantum mechanics that allows to quantify the degree of coupling between the spatial and polarisation degrees of freedom [39–41]. Experimentally, the VQF can be quantified directly from the Stokes parameters as [42, 43],

$$VQF = \sqrt{1 - \left(\frac{\mathbb{S}_1}{\mathbb{S}_0}\right)^2 - \left(\frac{\mathbb{S}_2}{\mathbb{S}_0}\right)^2 - \left(\frac{\mathbb{S}_3}{\mathbb{S}_0}\right)^2}, \quad (6)$$

where \mathbb{S}_i ($i = 0, 1, 2, 3$) is a number that results from integrating the Stokes parameters S_i over the entire transverse profile, i. e., $\mathbb{S}_i = \iint_{-\infty}^{\infty} S_i dA$. Figure 4 shows a

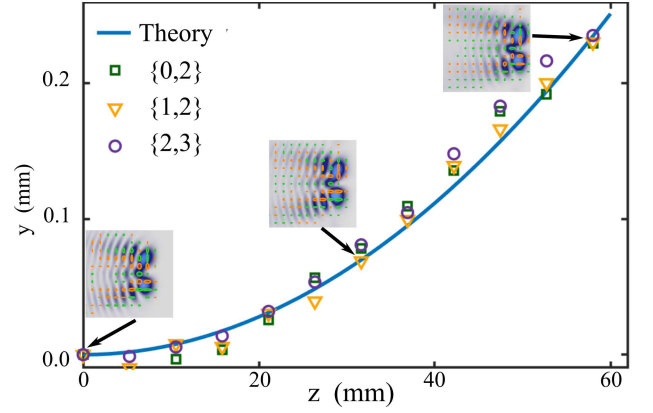


Fig. 3: Shift of the y -coordinate of the maximum intensity lobe position for three AVWs upon free-space propagation. The continuous curve represents the expected position predicted by the theory, whereas the data points correspond to experiment for the cases $\text{AVW}_{0,2}(\eta, \xi, z)$ (squares), $\text{AVW}_{1,2}(\eta, \xi, z)$ (triangles) and $\text{AVW}_{2,3}(\eta, \xi, z)$ (circles). Notice that all three cases accelerate in an identical way. Insets show the transverse polarisation distribution overlapped with the intensity profile of the $\text{AVW}_{1,2}(\eta, \xi, z)$ at three different planes.

representative example of the VQF as function of α for the specific case $\text{AVW}_{2,3}(\eta, \xi, z=0)$. As expected, the VQF increases from 0 to 1, as α increases from 0 to $\pi/4$ and then it decreases back to zero, as α reaches the value $\pi/2$. Insets show the intensity profile overlapped with the polarisation distribution for three key values, namely $\alpha = 0, \pi/4$ and $\pi/2$.

Finally, we analyse the polarisation states distribution of AVWs on the Poincaré sphere. It turns out that for a particular AVW all of them are mapped onto a great circle. Fig. 5(a) shows numerical simulations in the circular (top row) and horizontal/vertical linear (bottom row) bases. It can be seen that in the first case, the great circles intersect the North and South poles, meaning all polarisation states in the AVW are oriented at exactly the same polarisation angle and only differ in their ellipticity, containing all polarisation states from circular to linear. Interestingly, a change in the inter-modal phase β originates a rotation of the great circle around the S_3 axis (Fig. 5(a) top left panel), and a change in the weighting coefficient α causes the polarisation states location from complete to incomplete great circles, in such a way that the arc length is proportional to it (Fig. 5(a) top right panel). Similarly, in the case of horizontal/vertical linear polarisation basis (Fig. 5(a) bottom row), the great circles intersect the cross points between the S_1 axis and the sphere, and rotate around the S_1 axis when changing β . The effect of α is as in the circular basis. For instance, for $\alpha = \pi/2$ and $\beta = 0$, the polarisation distribution is

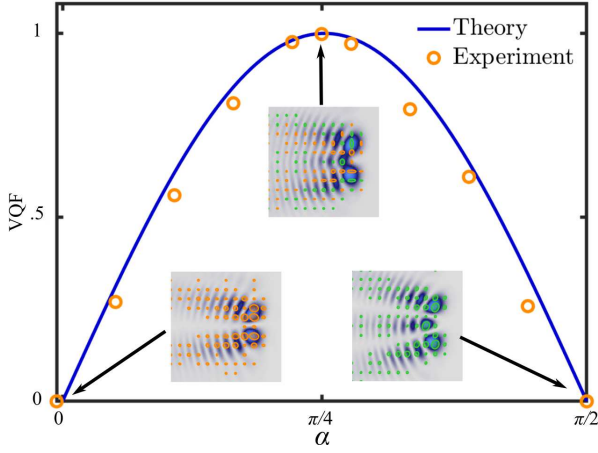


Fig. 4: Vector Quality Factor (VQF) as a function of the weighing coefficient $\alpha \in [0, \pi/2]$ for the mode $\mathbf{AVW}_{2,3}(\eta, \xi, z = 0)$. Insets show the intensity and polarisation distributions for $\alpha = 0, \pi/4$, and $\pi/2$.

mapped to the equator of the Poincaré sphere. For the case of circular polarisation basis, we corroborated this experimentally, as shown in Fig. 5(b), that shows a remarkable similarity to its theoretical counterpart. In summary, we have introduced theoretically and demonstrated experimentally a new family of vector beams with the ability to accelerate along parabolic trajectories upon free space propagation. Such accelerating beams differ quite dramatically from common vector beams, which always propagate along straight trajectories. These families of vector beams are constructed as a weighted superposition of the spatial and polarisation degrees of freedom carrying an inter-modal phase. To generate them, the spatial degree of freedom is encoded in a set of orthogonal solutions of the one-dimensional Schrödinger equation with a quartic potential, known as accelerating waves. An important feature of such modes is their propagation-invariant spatial and polarisation structures, as we corroborated experimentally. Further, the weighting coefficient allows tuning from purely scalar to completely vectorial, passing through intermediate states, which was also corroborated experimentally using the well-known measure of concurrence from quantum mechanics adapted for vector beams. Another important feature of these accelerating vector modes lies in their transverse polarisation distribution, which is mapped onto great circles on the Poincaré sphere. In particular, in the circular polarisation basis the great circles intersect the North and South poles, and contain states of polarisation from linear to circular, all with the same ellipticity angle. For comparison, cylindrical vector modes are mapped either to an equatorial line or to the whole Poincaré sphere (known as full-Poincaré

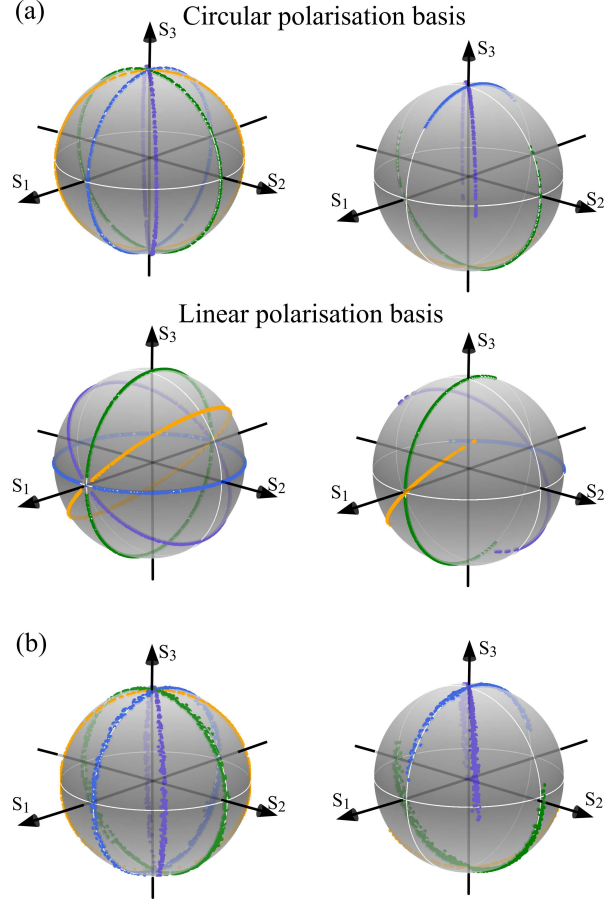


Fig. 5: Geometric representation on the Poincaré sphere of the transverse polarisation distribution of the vector mode $\mathbf{AVW}_{0,2}(\eta, \xi, z = 0)$. Left column shows modes with increasing values of the inter-modal phase, namely $\beta = 0$ (blue), $\beta = \pi/4$ (purple), $\beta = \pi/2$ (green) and $\beta = 3\pi/4$ (yellow). Right column shows modes with different weighting coefficients, namely $\alpha = \pi/12, \pi/6, \pi/3$ and $4\pi/12$, with the same inter-modal phases as in the left column for the sake of better visibility. (a) Theoretical results for the case of AVW in the circular (top row) and linear (bottom row) polarisation basis. (b) Corresponding experimental results for the case of the circular basis.

modes). Noteworthy, the inter-modal phase allows to rotate the circle of polarisation around the Poincaré sphere, leaving the points on North and South poles fixed. Given their interesting properties, we expect AVWs to find applications in fields such as optical manipulation, laser material processing, among others.

Funding: Consejo Nacional de Ciencia y Tecnología (PN2016-3140); National Natural Science Foundation of China (61975047).

References

- [1] Georgios A. Siviloglou and Demetrios N. Christodoulides. Accelerating finite energy Airy beams. *Opt. Lett.*, 32(8): 979–981, Apr 2007.
- [2] G. A. Siviloglou, J. Broky, A. Dogariu, and D. N. Christodoulides. Observation of Accelerating Airy Beams. *Phys. Rev. Lett.*, 99:213901, Nov 2007. 10.1103/PhysRevLett.99.213901. URL <https://link.aps.org/doi/10.1103/PhysRevLett.99.213901>.
- [3] Nikolaos K. Efremidis, Zhigang Chen, Mordechai Segev, and Demetrios N. Christodoulides. Airy beams and accelerating waves: an overview of recent advances. *Optica*, 6(5):686–701, May 2019.
- [4] Miguel A. Bandres. Accelerating parabolic beams. *Opt. Lett.*, 33(15):1678–1680, Aug 2008.
- [5] Miguel A. Bandres. Accelerating beams. *Opt. Lett.*, 34(24): 3791–3793, Dec 2009.
- [6] Elad Greenfield, Mordechai Segev, Wiktor Walasik, and Oren Raz. Accelerating light beams along arbitrary convex trajectories. *Phys. Rev. Lett.*, 106:213902, May 2011.
- [7] Peng Zhang, Yi Hu, Tongcang Li, Drake Cannan, Xiaobo Yin, Roberto Morandotti, Zhigang Chen, and Xiang Zhang. Nonparaxial Mathieu and Weber Accelerating Beams. *Phys. Rev. Lett.*, 109:193901, Nov 2012.
- [8] C Rosales-Guzmán, M Mazilu, J Baumgartl, V Rodríguez-Fajardo, R Ramos-García, and K Dholakia. Collision of propagating vortices embedded within Airy beams. *Journal of Optics*, 15(4):044001, apr 2013. 10.1088/2040-8978/15/4/044001.
- [9] Adrian Ruelas, Jeffrey A. Davis, Ignacio Moreno, Don M. Cottrell, and Miguel A. Bandres. Accelerating light beams with arbitrarily transverse shapes. *Opt. Express*, 22(3):3490–3500, Feb 2014.
- [10] Anatoly Patsyk, Miguel A. Bandres, Rivka Bekenstein, and Mordechai Segev. Observation of accelerating wave packets in curved space. *Phys. Rev. X*, 8:011001, Jan 2018. 10.1103/PhysRevX.8.011001. URL <https://link.aps.org/doi/10.1103/PhysRevX.8.011001>.
- [11] Parinaz Aleahmad, Mohammad-Ali Miri, Matthew S. Mills, Ido Kaminer, Mordechai Segev, and Demetrios N. Christodoulides. Fully Vectorial Accelerating Diffraction-Free Helmholtz Beams. *Phys. Rev. Lett.*, 109:203902, Nov 2012. 10.1103/PhysRevLett.109.203902. URL <https://link.aps.org/doi/10.1103/PhysRevLett.109.203902>.
- [12] Jeffrey A. Davis, Mark J. Mitry, Miguel A. Bandres, Isaac Ruiz, Kevin P. McAuley, and Don M. Cottrell. Generation of accelerating Airy and accelerating parabolic beams using phase-only patterns. *Appl. Opt.*, 48(17):3170–3176, 2009.
- [13] Andrew Forbes, Michael de Oliveira, and Mark R. Dennis. Structured light. *Nature Photonics*, 15(4):253–262, 2021. ISSN 1749-4893. 10.1038/s41566-021-00780-4. URL <https://doi.org/10.1038/s41566-021-00780-4>.
- [14] Halina Rubinsztein-Dunlop, Andrew Forbes, M. V. Berry, M. R. Dennis, David L. Andrews, Masud Mansuripur, Cornelia Denz, Christina Alpmann, Peter Banzer, and Thomas Bauer. Roadmap on structured light. *J. Opt.*, 19(1):013001, 2017.
- [15] Carmelo Rosales-Guzmán, Bienvenu Ndagano, and Andrew Forbes. A review of complex vector light fields and their applications. *J. Opt.*, 20(12):123001, 2018.
- [16] Thomas Konrad and Andrew Forbes. Quantum mechanics and classical light. *Contemporary Physics*, pages 1–22, 2019.
- [17] J H Eberly, Xiao-Feng Qian, Asma Al Qasimi, Hazrat Ali, M A Alonso, R Gutiérrez-Cuevas, Bethany J Little, John C Howell, Tanya Malhotra, and A N Vamivakas. Quantum and classical optics—emerging links. *Phys. Scr*, 91(6):063003, 2016. URL <http://stacks.iop.org/1402-4896/91/i=6/a=063003>.
- [18] Ermes Toninelli, Bienvenu Ndagano, Adam Vallés, Bereneice Sephton, Isaac Nape, Antonio Ambrosio, Federico Capasso, Miles J Padgett, and Andrew Forbes. Concepts in quantum state tomography and classical implementation with intense light: a tutorial. *Advances in Optics and Photonics*, 11(1): 67–134, 2019.
- [19] Andrew Forbes, Andrea Aiello, and Bienvenu Ndagano. Classically entangled light. In *Progress in Optics*, pages 99–153. Elsevier Ltd., 2019.
- [20] Falk Töppel, Andrea Aiello, Christoph Marquardt, Elisabeth Giacobino, and Gerd Leuchs. Classical entanglement in polarization metrology. *New J. Phys.*, 16(7):073019, 2014.
- [21] Xiao-Bo Hu, Bo Zhao, Zhi-Han Zhu, Wei Gao, and Carmelo Rosales-Guzmán. In situ detection of a cooperative target’s longitudinal and angular speed using structured light. *Opt. Lett.*, 44(12):3070–3073, Jun 2019. 10.1364/OL.44.003070.
- [22] Stefan Berg-Johansen, Falk Töppel, Birgit Stiller, Peter Banzer, Marco Ornigotti, Elisabeth Giacobino, Gerd Leuchs, Andrea Aiello, and Christoph Marquardt. Classically entangled optical beams for high-speed kinematic sensing. *Optica*, 2(10):864–868, Oct 2015. 10.1364/OPTICA.2.000864.
- [23] B. Ndagano, I. Nape, M. A. Cox, C. Rosales-Guzmán, and A. Forbes. Creation and detection of vector vortex modes for classical and quantum communication. *J. Light. Technol.*, 36(2):292–301, Jan 2018. 10.1109/JLT.2017.2766760.
- [24] Bienvenu Ndagano, Benjamin Perez-Garcia, Filippus N. Roux, Melanie McLaren, Carmelo Rosales-Guzmán, Yingwen Zhang, Othmane Mouane, Raul I. Hernandez-Aranda, Thomas Konrad, and Andrew Forbes. Characterizing quantum channels with non-separable states of classical light. *Nature Phys.*, 13:397–402, 2017.
- [25] E. Otte and C. Denz. Optical trapping gets structure: Structured light for advanced optical manipulation. *Applied Physics Reviews*, 7(4):041308, 2020.
- [26] Alicia Sit, Frédéric Bouchard, Robert Fickler, Jérémie Gagnon-Bischoff, Hugo Larocque, Khabat Heshami, Dominique Elser, Christian Peuntinger, Kevin Günthner, Bettina Heim, Christoph Marquardt, Gerd Leuchs, Robert W. Boyd, and Ebrahim Karimi. High-dimensional intracity quantum cryptography with structured photons. *Optica*, 4(9): 1006–1010, Sep 2017. 10.1364/OPTICA.4.001006. URL <http://www.osapublishing.org/optica/abstract.cfm?URI=optica-4-9-1006>.
- [27] Q. Zhan. Cylindrical vector beams: from mathematical concepts to applications. *Adv. Opt. Photonics*, 1:1–57, 2009.
- [28] Angela Dudley, Yanming Li, Thandeka Mhlanga, Michael Escuti, and Andrew Forbes. Generating and measuring

- nondiffracting vector Bessel beams. *Opt. Lett.*, 38:3429–3432, 2013.
- [29] Eileen Otte and Cornelia Denz. Sculpting complex polarization singularity networks. *Opt. Lett.*, 43(23):5821–5824, Dec 2018. 10.1364/OL.43.005821.
- [30] Yao-Li, Xiao-Bo Hu, Benjamin Perez-Garcia, Bo-Zhao, Wei Gao, Zhi-Han Zhu, and Carmelo Rosales-Guzmán. Classically entangled Ince–Gaussian modes. *Applied Physics Letters*, 116(22):221105, 2020. 10.1063/5.0011142.
- [31] Carmelo Rosales-Guzmán, XiaoBo Hu, Valeria Rodríguez-Fajardo, Raul Ignacio Hernandez-Aranda, Andrew Forbes, and Benjamin Perez-Garcia. Experimental generation of Helical Mathieu-Gauss vector modes. *Journal of Optics*, 2021.
- [32] Keshaan Singh, Wagner Tavares Buono, Andrew Forbes, and Angela Dudley. Accelerating polarization structures in vectorial fields. *Opt. Express*, 29(2):2727–2737, Jan 2021. 10.1364/OE.411029.
- [33] Junxiao Zhou, Yachao Liu, Yougang Ke, Hailu Luo, and Shuangchun Wen. Generation of Airy vortex and Airy vector beams based on the modulation of dynamic and geometric phases. *Opt. Lett.*, 40(13):3193–3196, 2015.
- [34] K. Banerjee, S. P. Bhatnagar, V. Choudhry, S. S. Kanwal, and David Robert Bates. The anharmonic oscillator. *Proceedings of the Royal Society of London. A. Mathematical and Physical Sciences*, 360(1703):575–586, 1978. 10.1098/rspa.1978.0086. URL <https://royalsocietypublishing.org/doi/abs/10.1098/rspa.1978.0086>.
- [35] T. A Driscoll, N. Hale, and L. N. Trefethen. *Chebfun Guide*. Pafnuty Publications, 2014. URL <http://www.chebfun.org/docs/guide/>.
- [36] Jeffrey A. Davis, Mark J. Mitry, Miguel A. Bandres, and Don M. Cottrell. Observation of accelerating parabolic beams. *Opt. Express*, 16(17):12866–12871, Aug 2008. 10.1364/OE.16.012866. URL <http://www.opticsexpress.org/abstract.cfm?URI=oe-16-17-12866>.
- [37] Carmelo Rosales-Guzmán, Xiao-Bo Hu, Adam Selyem, Pedro Moreno-Acosta, Sonja Franke-Arnold, Ruben Ramos-Garcia, and Andrew Forbes. Polarisation-insensitive generation of complex vector modes from a digital micromirror device. *Scientific Reports*, 10(1):10434, 2020. 10.1038/s41598-020-66799-9.
- [38] Xiao-Bo Hu, Benjamin Perez-Garcia, Valeria Rodríguez-Fajardo, Raul I. Hernandez-Aranda, Andrew Forbes, and Carmelo Rosales-Guzmán. Free-space local nonseparability dynamics of vector modes. *Photon. Res.*, 9(4):439–445, 2021. 10.1364/PRJ.416342.
- [39] Melanie McLaren, Thomas Konrad, and Andrew Forbes. Measuring the nonseparability of vector vortex beams. *Phys. Rev. A*, 92:023833, 2015.
- [40] Bienvenu Ndagano, Robert Brüning, Melanie McLaren, Michael Duparré, and Andrew Forbes. Fiber propagation of vector modes. *Opt. Express*, 23:17330–17336, 2015. 10.1364/OE.23.017330.
- [41] Bo Zhao, Xiao-Bo Hu, Valeria Rodríguez-Fajardo, Zhi-Han Zhu, Wei Gao, Andrew Forbes, and Carmelo Rosales-Guzmán. Real-time stokes polarimetry using a digital micromirror device. *Opt. Express*, 27(21):31087–31093, Oct 2019. 10.1364/OE.27.031087.
- [42] Adam Selyem, Carmelo Rosales-Guzmán, Sarah Croke, Andrew Forbes, and Sonja Franke-Arnold. Basis-independent tomography and nonseparability witnesses of pure complex vectorial light fields by Stokes projections. *Phys. Rev. A*, 100:063842, Dec 2019. 10.1103/PhysRevA.100.063842.
- [43] Amogh Manthalkar, Isaac Nape, Najmeh Tabe Bordbar, Carmelo Rosales-Guzmán, Shanti Bhattacharya, Andrew Forbes, and Angela Dudley. All-digital Stokes polarimetry with a digital micromirror device. *Opt. Lett.*, 45(8):2319–2322, Apr 2020.